JOURNAL OF AIRCRAFT
Vol. 47, No. 6, November–December 2010

Inverse Aerodynamic Design Procedure for Propellers Having a Prescribed Chord-Length Distribution

Martin Hepperle*
DLR, German Aerospace Center, 38108 Braunschweig, Germany

DOI: 10.2514/1.46535

Inverse design methods are elegant and efficient tools for the design of aerodynamic shapes like airfoils, wings, and propellers. In the case of propeller design, only a few general parameters have to be prescribed and the design procedure returns the propeller geometry in terms of chord-length and blade-angle distributions along the radius. The common design procedures require the prescription of the lift coefficient over the blade radius in order to obtain the unknown chord length. In this paper, a modified design method is presented that allows for designing optimum propellers having a prescribed chord-length distribution. Now the radial distribution of the lift coefficient becomes the unknown, which is determined by the design procedure.

Nomenclature

a	=	axial induction factor
a'	=	tangential induction factor
B	=	number of blades
C_d	=	local drag coefficient
C_ℓ	=	local lift coefficient
C_P	=	power coefficient, $P/(\rho_\infty \cdot n^3 \cdot D^5)$
C_T	=	thrust coefficient, $T/(\rho_\infty \cdot n^2 \cdot D^4)$
c	=	local chord length
D	=	propeller diameter
G	=	Goldstein function
H	=	pitch height, v_∞/n
n	=	number of revolutions per second
P	=	power
R	=	propeller radius
Re	=	Reynolds number
r	=	radial coordinate
T	=	thrust
T_c	=	thrust coefficient, $(2 \cdot T)/(\rho_\infty \cdot v_\infty^2 \cdot \pi \cdot R^2)$
t	=	thickness
v_∞	=	flight speed
w_i	=	induced velocity
α	=	local angle of attack
β	=	blade angle
Γ	=	local circulation strength
Δv	=	induced axial velocity
δ	=	local swirl angle
η	=	propulsive efficiency
λ	=	advance ratio, $v_\infty/(\Omega \cdot R)$
ρ_∞	=	density of air
ϕ	=	local inflow angle
Ω	=	angular velocity

Introduction

THE theory of optimum propellers, having maximum efficiency, has been developed early in the 20th century ([1–3]). The optimum condition requires the axial displacement velocity of the vortex sheet shed by the propeller blades to be constant over the radius. This theory has successfully been applied to propeller design using the then already available blade-element methods [4]. These methods link axial and circumferential momentum considerations with the local circulation strength to solve for the downwash induced by the propeller on itself. The influence of the trailing wakes and the finite number of blades is usually approximated to avoid the complex calculation of accurate influence coefficients. Despite these simplifications, the results obtained from the blade-element momentum methods are astonishingly accurate and very useful for the preliminary design and optimization of propellers. While the blade-element momentum method has been used continuously since the 1930s for the analysis task, the procedures for the inverse design of optimum propellers were less known and have been rediscovered only in the 1970s. To design propellers having minimum energy loss, Larrabee [5] applied the theory to formulate a straightforward design procedure. Later, the accuracy of the design method was improved by Adkins and Liebeck [6,7] by also removing a light-loading assumption so that design and analysis produced identical results. A comprehensive survey of the development of propeller theory can be found in [8].

The optimum design procedure is usually applied in the following way: the user initiates the design by prescribing five global parameters of diameter D, air speed v_∞, speed of rotation n, total power P, or thrust T, and the number of blades B. Additionally, he has to define the distribution of the local lift coefficient $C_\ell = f(r/R)$ and the corresponding local angle of attack $\alpha = f(r/R)$ along the radius of the propeller. The design method then returns the distributions of the chord length $c = f(r/R)$ and the blade angle $\beta = f(r/R)$ for a propeller fulfilling the condition of maximum efficiency.

Recently, the author had to solve a slightly different design task: *find the optimum propeller for a given distribution of the chord length*. In this case, the inverse design procedure must generate the distribution of the local lift coefficient $C_\ell = f(r/R)$ as well as the local blade angle $\beta = f(r/R)$ (see Fig. 1).

The core relation of the classical design method which connects chord length and lift coefficient is the match of the momentum and the local circulation strength:

$$C_\ell \cdot \frac{c}{R} \cdot v_{\text{eff}} \cdot B = 4 \cdot \pi \cdot \lambda \cdot G \cdot v_\infty \cdot \zeta \tag{1}$$

where v_{eff} is the flow velocity, as depicted in Fig. 2, and the displacement velocity ratio ζ is described below. It can be seen that the local lift coefficient C_ℓ and the local chord length c/R occur on the left side of Eq. (1) and are therefore exchangeable. Thus, it is possible to prescribe the chord length in order to obtain the lift coefficient instead of prescribing the lift coefficient to obtain the chord length as was done in the classical application.

Design Procedure

For optimum propellers having minimum energy loss the axial displacement velocity ratio $\zeta = (v_\infty + \Delta v)/v_\infty$ must be constant

Received 29 July 2009; revision received 13 August 2010; accepted for publication 23 August 2010.

*Institute of Aerodynamics and Flow Technology.

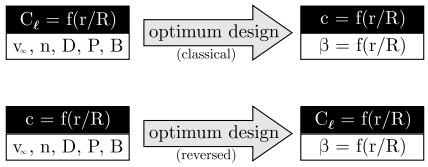

Fig. 1 Input and output parameters for the classical and the reversed design procedure.

along the radius, but its value is unknown. An iterative solver is used to determine the value of ζ, depending on blade geometry, local inflow conditions, and the airfoil characteristics.

For realistic applications the nonlinear aerodynamic characteristics of the airfoil sections are specified in tabular form, because no analytical relationship exists between the angle of attack and the lift (respectively, the drag coefficient). Therefore, an additional iteration is introduced to solve for the unknown lift coefficient. Note that because of the limitation of the maximum lift coefficient due to stall, ill-posed cases do exist when the user is asking for too-narrow blades for a given airfoil section.

The overall design procedure closely follows the process described in [6,7] and is outlined below, including the required modifications. It is possible to specify either thrust or power or torque. If the thrust is given, we perform the following steps:

First, the five design variables v_∞, Ω, R, B, and T and the chord-length distribution $c/R = f(r/R)$ must be prescribed. Additionally, the radial distribution of airfoil sections and their aerodynamic characteristics must be defined. These parameters form the complete set of input parameters.

The design process starts with the determination of the thrust coefficient

$$T_c = \frac{2 \cdot T}{\rho_\infty \cdot v_\infty^2 \cdot \pi \cdot R^2} \tag{2}$$

and the advance ratio:

$$\lambda = \frac{v_\infty}{\Omega \cdot R} \tag{3}$$

Next, we begin an outer iteration to solve for the unknown displacement velocity ratio ζ by selecting an initial value: e.g., $\zeta = \zeta^{(i)} = 0$.

The inflow angle at the propeller tip is determined from

$$\phi_{\text{tip}} = \arctan(\lambda \cdot (1 + \zeta^{(i)}/2)) \tag{4}$$

For each radial station $\xi = r/R$ we also calculate the local inflow angle from

$$\phi = \arctan\left(\frac{\lambda}{\xi} \cdot \left(1 + \frac{\zeta^{(i)}}{2}\right)\right) \tag{5}$$

The tip loss function can be approximated, for example, by Prandtl's analytical expression with

$$F = (2/\pi) \cdot \arccos(e^{-f}) \tag{6}$$

and

$$f = (B/2) \cdot (1 - \xi)/\sin\phi_{\text{tip}} \tag{7}$$

to determine an approximation of the Goldstein function

$$G = F \cdot \sin\phi \cdot \cos\phi \tag{8}$$

To solve for the unknown lift coefficient C_ℓ we start an inner iteration by selecting an initial value $C_\ell^{j=0}$. The local airfoil characteristics are used to find the corresponding angle of attack $\alpha^{(j)}$ and the drag coefficient $C_d^{(j)}$.

The axial induction factor is

$$a = \zeta^{(i)}/2 \cdot \cos^2\phi \cdot (1 - C_d^{(j)}/C_\ell^{(j)} \cdot \tan\phi) \tag{9}$$

and the tangential induction factor becomes

$$a' = (\zeta^{(i)}/2) \cdot \lambda/(r/R) \cdot \cos\phi \cdot \sin\phi \cdot (1 + C_d^{(j)}/(C_\ell^{(j)} \cdot \tan\phi)) \tag{10}$$

We can now calculate the local inflow velocity at the blade section

$$v_{\text{eff}} = \frac{v_\infty \cdot (1 + a)}{\sin\phi} \tag{11}$$

to find a new lift coefficient

$$C_\ell^{(j+1)} = (4 \cdot \pi \cdot \lambda \cdot G \cdot v_\infty \cdot \zeta^{(i)})/(v_{\text{eff}} \cdot (c/R) \cdot B) \tag{12}$$

This inner iteration is performed until $|C_\ell^{(j+1)} - C_\ell^{(j)}| < \varepsilon$.

Finally, following the procedure according to [5], two local derivatives for this blade element are determined from

$$\partial I_1/\partial\xi = 4 \cdot \xi \cdot G \cdot (1 - C_d/C_\ell \cdot \tan\phi) \tag{13}$$

and

$$\partial I_2/\partial\xi = \lambda \cdot 2 \cdot G \cdot (1 - C_d/C_\ell \cdot \tan\phi) \cdot (1 + C_d/C_\ell/\tan\phi) \cdot \sin\phi \cdot \cos\phi \tag{14}$$

The evaluation of Eqs. (5–14) is performed for each blade element. When this process is complete, the derivatives [Eqs. (13) and (14)] are integrated from hub to tip:

$$I_1 = \int_{\xi_{\text{hub}}}^{1} (\partial I_1/\partial\xi) \cdot \mathrm{d}\xi \tag{15}$$

$$I_2 = \int_{\xi_{\text{hub}}}^{1} (\partial I_2/\partial\xi) \cdot \mathrm{d}\xi \tag{16}$$

With the thrust coefficient according to Eq. (2) we can finally determine a new approximation for the displacement velocity ζ:

$$\zeta^{(i+1)} = I_1/(2 \cdot I_1) - \sqrt{(I_1/(2 \cdot I_1))^2 - T_c/I_2} \tag{17}$$

The outer iteration is continued with Eq. (4) using the new value until $|\zeta^{(i+1)} - \zeta^{(i)}| < \varepsilon$. Finally, all the desired quantities can be calculated as usual (see [6,7]). This design procedure was integrated into the author's computer program PROPPY, which contains a variety of functions for the design, analysis, and manipulation of propellers and has been used successfully for several propeller designs.[†] The next section presents three example applications of the design method.

Applications

Example 1: Generic Test Cases

As a demonstration of the capability of the redesign procedure, two ideal test cases have been defined. To exclude the effect of airfoil lift and drag characteristics, an ideal airfoil was defined for this test. It had a constant ratio of $C_\ell/C_d = 100$, independent of the lift coefficient.

Using this fictitious airfoil, two designs were performed: design A for a prescribed constant lift coefficient $C_\ell(r) = 0.75$ (following the classical inverse design procedure) and design B for a prescribed constant chord length $c(r) = 0.125$ using the new design procedure. The value for the chord length was chosen to be close to the chord length at 75% of the radius of the first design, which avoided setting up an ill-posed design problem.

The geometry returned by each design procedure is presented in the form of the distributions of the chord-length ratio c/R, the blade angle β, and the pitch-to-diameter ratio H/D in Figs. 3–5. It can be

[†]Information available online at http://www.grob-aircraft.eu, http://www.lange-flugzeugbau.com, and http://www.solarimpulse.com [retrieved 27 June 2010].

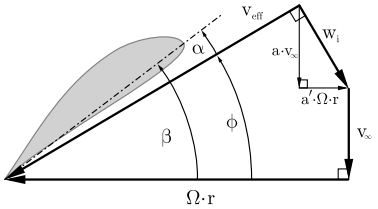

Fig. 2 Inflow at a section of the propeller blade.

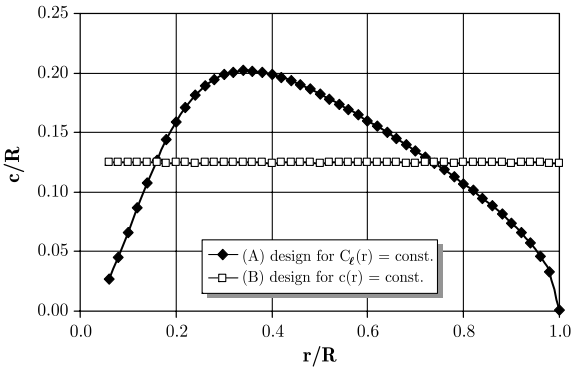

Fig. 3 Chord length distributions for both test cases.

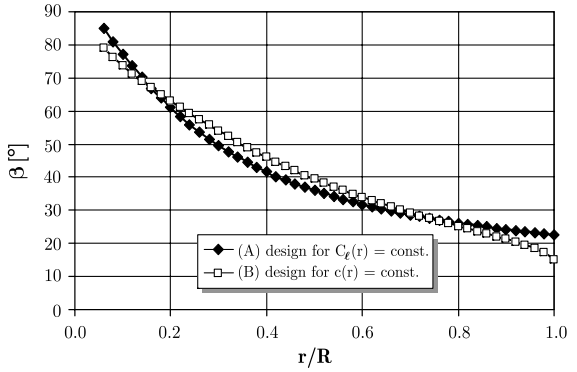

Fig. 4 Distribution of the blade angle for the test cases.

seen that the different chord-length distributions also lead to a different distribution of the local blade angle. Compared to design A the prescribed chord length of design B is larger at the tip and at the root. In case B, the same optimum circulation distribution (depicted in Fig. 6) is achieved by a reduction of the local blade angle toward root and tip. In their design point, both propellers induce the same velocities on the onset flowfield and hence produce the same optimum distribution of the swirl angle, as shown in Fig. 7. The main

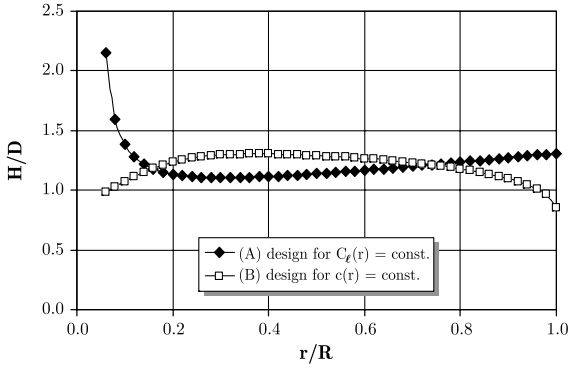

Fig. 5 Distribution of the pitch-to-diameter ratio for both test cases.

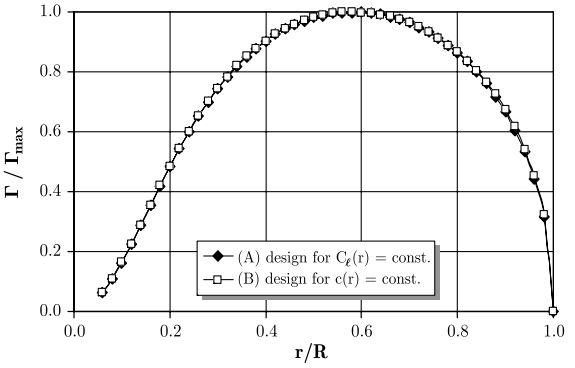

Fig. 6 Distribution of the normalized circulation for both test cases.

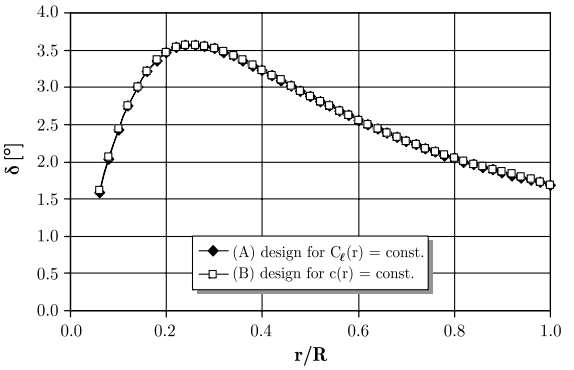

Fig. 7 Distribution of the swirl angle immediately behind the propeller for both test cases.

difference can be observed in the radial distributions of the lift coefficient (Fig. 8). Because of the constant $C_\ell/C_d = 100$ airfoil sections the offdesign analysis yields almost identical results for thrust and power coefficients (Fig. 9) and therefore for the efficiency (Fig. 10). The offdesign performance is slightly different, due to the differences in geometry. When the constant C_ℓ/C_d airfoil is replaced by a realistic airfoil, the differences in offdesign performance will become larger. For a realistic design one would select or design the airfoil sections so that they operate close to their maximum lift coefficient and provide acceptable offdesign performance (see [5–7] for more aspects of practical propeller design).

Example 2: Redesign of a Historic Aircraft Propeller

To preserve the few genuine samples of early aviation, replica aircraft are built. These follow the external lines of the original but are often modified to improve airworthiness and safety. The original powerplants can also be substituted for modern, more reliable, and serviceable engines. Unfortunately, these new engines usually deliver their power at higher rpm than the original engines. The

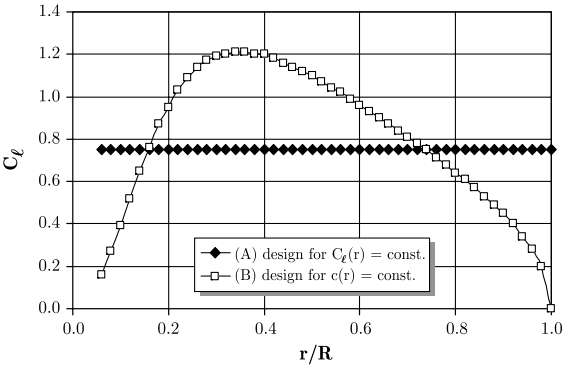

Fig. 8 Distribution of the lift coefficient for the test cases.

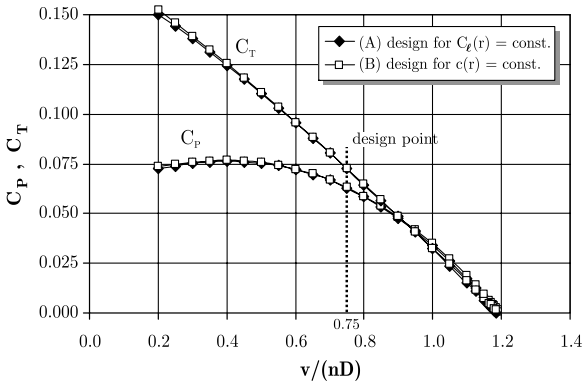

Fig. 9 Thrust and power coefficients versus advance ratio for both test cases.

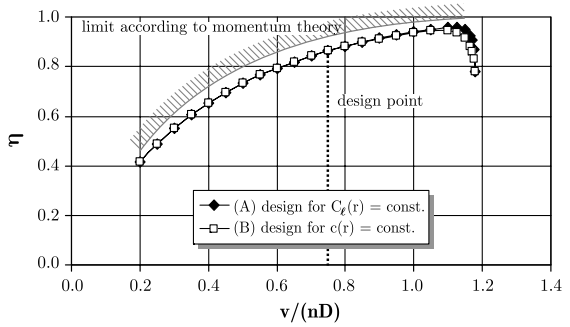

Fig. 10 Efficiency versus advance ratio for both test cases. The limit curve assumes the same thrust loading.

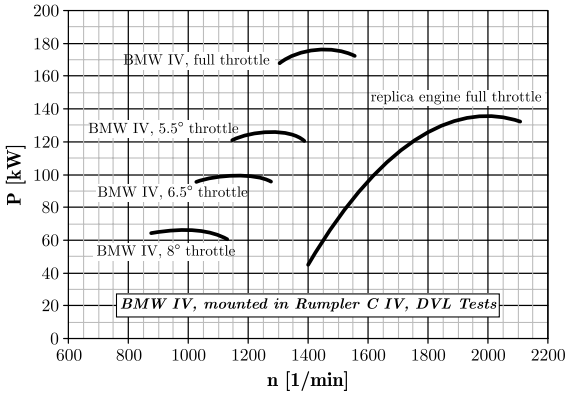

Fig. 11 Power curves of the BMW IV engine at different throttle settings compared to the engine used for the Fokker D VII replica aircraft.

author was asked to develop a propeller for a Fokker D VII replica aircraft to be equipped with a Gipsy Queen 30 MK 2 inline engine. The original Fokker D VII series aircraft had been powered by water-cooled Mercedes D-III six-cylinder inline engines, which produced about 130 to 180 kW at 1400 rpm. The corresponding wooden propellers typically had a diameter of 2.75 to 2.8 m and a pitch height of 2.05 to 2.35 m.

The modified replacement engine delivers the required power at speeds of about 2000 rpm (Fig. 11). The new propeller design had to match the characteristics of the replacement engine but, at the same time, had to maintain the planform of the original propeller for authentic looks.

For comparison, the geometry of an original propeller sample was measured at 10 radial stations. This measurement had to be made in situ at a museum and was therefore of relatively low accuracy.

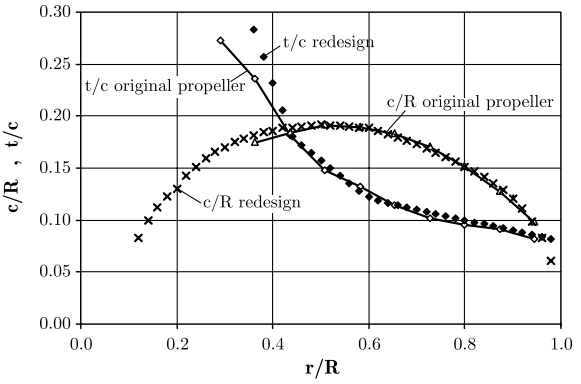

Fig. 12 Distributions of relative chord length and relative thickness of the Fokker D VII propellers.

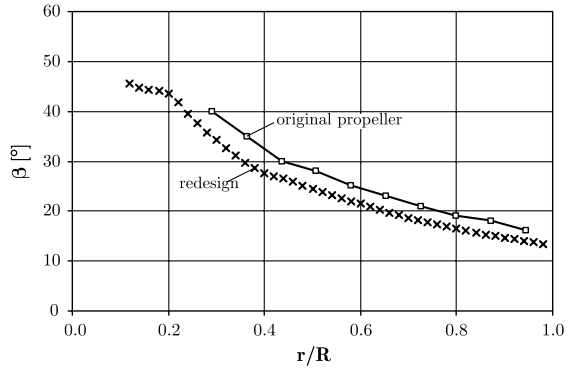

Fig. 13 Distribution of the blade angle of the original and the redesigned Fokker D VII propeller.

More details can be found in Fig. 12, which depicts the radial distributions of the chord length $c/R = f(r/R)$ and the relative thickness $t/c = f(r/R)$ of the original and the redesigned propeller. It can be seen that the redesign matches the original very well. The thickness distribution was preserved by selection of appropriate airfoil sections in order to achieve similar stiffness and mass properties for the both propellers. The distribution of the blade angle, as presented in Fig. 13, shows the expected difference: due to the higher rpm of the redesigned propeller, its blade angle must be considerably lower.

Example 3: Redesign of a Generic High-Speed Propeller

A performance model of modern high-speed propellers was needed for research studies of future aircraft configurations. Such aircraft require propellers capable of consuming about 5000 kW in cruise and about 8000 kW at takeoff. Unfortunately, performance maps of modern propellers are generally not freely available. Therefore, a redesign of such a propeller was performed. The main parameters for the propeller design are listed in Table 1. Figure 14 shows the airfoil sections which have been used to determine the airfoil characteristics.

Table 1 Design parameters of the high-speed propeller

Parameter	Symbol	Value	Unit
Number of blades	B	8	——
Diameter	D	5.0	m
Spinner diameter	D_s	1.0	m
Rotational speed	n	850	1/ min
Cruise speed	v	200	m/s
Cruise altitude	H	9000	m
Shaft power	P	8800	kW

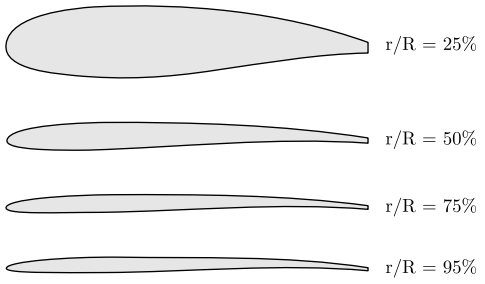

Fig. 14 Airfoil sections used for high-speed propeller.

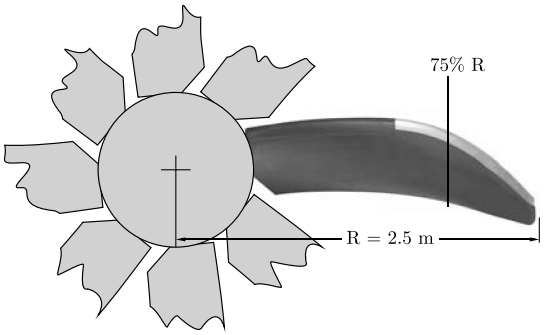

Fig. 15 Front view of sample blade used for the reconstruction of the high-speed propeller.

To produce a realistic state-of-the-art design, the geometry of a typical propeller was derived from available photographs. The chord-length distribution was extracted from a photograph looking at a sample propeller blade normal to the 75% radius station (Fig. 15).

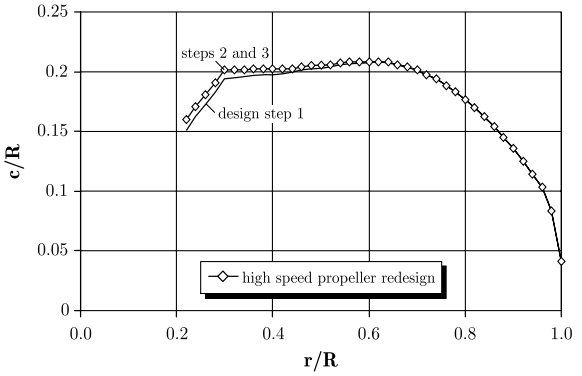

Fig. 16 Distribution of chord length of the redesigned high-speed propeller.

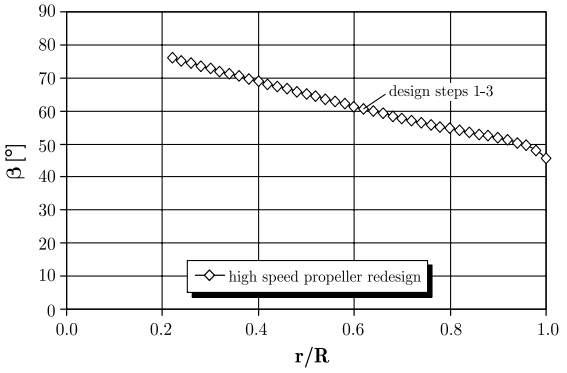

Fig. 17 Distribution of blade angle of the redesigned high-speed propeller. The difference between the design steps is smaller than 0.05°.

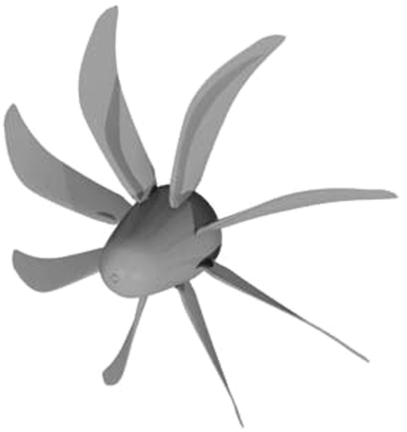

Fig. 18 Geometry of redesigned high-speed propeller.

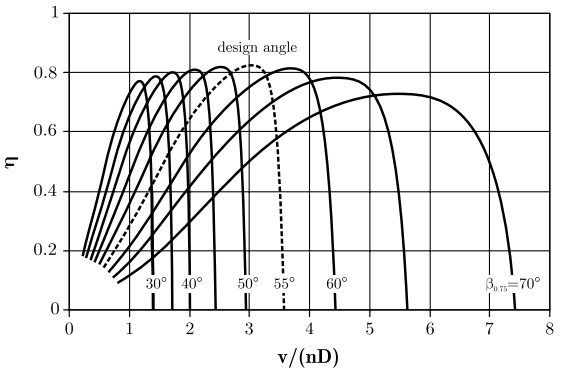

Fig. 19 Efficiency versus advance ratio of the redesigned high-speed propeller.

The outline of the blade can be measured with sufficient accuracy from such a photograph.

Because such a view shows the projected chord length $c^* = c \cdot \cos(\beta - \beta_{0.75})$ and not the true chord length, an iteration of the unknown blade angle must be performed. High-speed propellers operate at high advance ratios, and so the blades have a relatively small amount of twist from root to tip. Therefore, the projected chord length, as shown in Fig. 15, looking normal to the blade at 75% of the radius is already very close to the true chord-length distribution. For the first redesign step it was assumed that the blade twist is zero: i.e., the blade angle $\beta(r/R) = \beta_{0.75}$ and hence $c = c^*$. Then the redesign was repeated using the calculated distribution of $\beta(r/R)$ obtained from the first redesign step. The practical application shows that one or two iterations are sufficient to produce a final geometry with converged distributions of chord length and blade angle.

Figures 16 and 17 present the distributions of chord length and blade angle, and Fig. 18 shows a view of the complete propeller. To allow the approximate modeling of the aerodynamic characteristics of such high-speed propellers, the PROPPY code optionally modifies the given airfoil properties by applying local sweep and Mach number corrections. Alternatively, the user provides airfoil data that account for local Mach number, sweep, and cascade effects. It is obvious that offdesign flows with strong shocks cannot be handled accurately by this approach, but the results are valid for the regime around the design point of a well-designed propeller.

The analysis of the designed propeller at different blade angles is presented in the form of efficiency versus advance ratio in Fig. 19.

Conclusions

A new application of an inverse design method for propellers was presented. It produces optimum propellers having minimum induced loss. In contrast to existing methods, the procedure uses a prescribed chord-length distribution to produce the distributions of blade angle

and lift coefficient as required to maximize efficiency. Such a method is useful for the redesign of existing propellers and for the design of propellers or fans that are constrained by available space or manufacturing methods. The algorithm has successfully been applied to several redesign tasks, ranging from historic replica propellers to recent high-speed propellers. Future refinements of the method will include a combination of the design methods so that it becomes possible to prescribe the chord length over one part of the blade and the lift coefficient over the remaining part. This would allow considering local constraints such as a required root or tip chord length.

References

[1] Betz, A., "Schraubenpropeller mit Geringstem Energieverlust," *Nachrichten der Königlichen Gesellschaft der Wissenschaften zu Göttingen, Mathematisch-Physikalische Klasse*, Akademie der Wissenschaften in Göttingen, Göttingen, Germany, 1919, pp. 193–217.

[2] Prandtl, L., and Betz, A., *Vier Abhandlungen zur Hydrodynamik und Aerodynamik*, Kaiser-Wilhelm-Gesellschaft, Göttingen, Germany, 1927, pp. 68–92.

[3] Goldstein, S., "On the Vortex Theory of Screw Propellers," *Proceedings of the Royal Society of London*, Vol. 123, 1929, pp. 440–465. doi:10.1098/rspa.1929.0078

[4] Helmbold, H. B., "Der Entwurf einer Luftschraube für Gegebene Betriebsverhältnisse," *Ringbuch der Luftfahrttechnik*, Vol. 1, edited by W. Hoff, DVL, Berlin, 1937, Chap. 1C2.

[5] Larrabee, E., "Practical Design of Minimum Induced Loss Propellers," *Business Aircraft Meeting and Exposition*, Society of Automotive Engineers, Warrendale, PA, April 1979, Paper 790585.

[6] Adkins, N., and Liebeck, R. H., "Design of Optimum Propellers," *Journal of Propulsion and Power*, Vol. 10, No. 5, 1994, pp. 676–682. doi:10.2514/3.23779

[7] Adkins, N., and Liebeck, R. H., "Design of Optimum Propellers," 21st Aerospace Sciences Meeting, Reno, NV, AIAA Paper 83-0190, Jan. 1983.

[8] Wald, Q. R., "The Aerodynamics of Propellers," *Progress in Aerospace Sciences*, Vol. 42, 2006, pp. 85–128. doi:10.1016/j.paerosci.2006.04.001